

# Multifunctional pH sensitive 3D scaffolds for treatment and prevention of bone infection

Mónica Cicuéndez<sup>a, b</sup>, Juan C. Doadrio<sup>a</sup>, Ana Hernández<sup>a</sup>, M. Teresa Portolés<sup>c</sup>, Isabel Izquierdo-Barba<sup>a, b, \*</sup>,  
María Vallet-Regí<sup>a, b, \*</sup>

<sup>a</sup> Departamento de Química Inorgánica y Bioinorgánica, Facultad de Farmacia, Universidad Complutense de Madrid, Instituto de Investigación Sanitaria Hospital 12 de Octubre i+12, Plaza Ramón y Cajal s/n, 28040 Madrid, Spain

<sup>b</sup> CIBER de Bioingeniería, Biomateriales y Nanomedicina, CIBER-BBN, Madrid, Spain

<sup>c</sup> Departamento de Bioquímica and Biología Molecular I, Facultad de Ciencias Químicas, Universidad Complutense de Madrid, Instituto de Investigación Sanitaria San Carlos IdISSC, Ciudad Universitaria s/n, 28040 Madrid, Spain

## ARTICLE INFO

### Article history:

Received 1 August 2017

Received in revised form 16 October 2017

Accepted 7 November 2017

Available online xxx

### Keywords:

3D scaffolds

Levofloxacin

pH-dependent release

Biofilm

*S. aureus*

Biocompatibility

Co-culture assays

## ABSTRACT

Multifunctional-therapeutic three-dimensional (3D) scaffolds have been prepared. These biomaterials are able to destroy the *S. aureus* bacterial *biofilm* and to allow bone regeneration at the same time. The present study is focused on the design of pH sensitive 3D hierarchical meso-macroporous 3D scaffolds based on MGHA nanocomposite formed by a mesostructured glassy network with embedded hydroxyapatite nanoparticles, whose mesopores have been loaded with levofloxacin (Levo) as antibacterial agent. These 3D platforms exhibit controlled and pH-dependent Levo release, sustained over time at physiological pH (7.4) and notably increased at infection pH (6.7 and 5.5), which is due to the different interaction rate between diverse Levo species and the silica matrix. These 3D systems are able to inhibit the *S. aureus* growth and to destroy the bacterial *biofilm* without cytotoxic effects on human osteoblasts and allowing an adequate colonization and differentiation of preosteoblastic cells on their surface. These findings suggest promising applications of these hierarchical MGHA nanocomposite 3D scaffolds for the treatment and prevention of bone infection.

### Statement of Significance

Multifunctional 3D nanocomposite scaffolds with the ability for loading and sustained delivery of an antimicrobial agent, to eliminate and prevent bone infection and at the same time to contribute to bone regeneration process without cytotoxic effects on the surrounding tissue has been proposed. These 3D scaffolds exhibit a sustained levofloxacin delivery at physiological pH (pH 7.4), which increasing notably when pH decreases to characteristic values of bone infection process (pH 6.7 and pH 5.5). *In vitro* competitive assays between preosteoblastic and bacteria onto the 3D scaffold surface demonstrated an adequate osteoblast colonization in entire scaffold surface together with the ability to eliminate bacteria contamination.

© 2017.

## 1. Introduction

Osteomyelitis (OM) is a bone infection with very important clinical and socio-economic implications, which is mainly caused by the pathogen *Staphylococcus aureus* (*S. aureus*). OM results in inflammatory reaction that leads to bone destruction (osteolysis), being extremely difficult to treat and may lead to patient death [1–4]. Bacteria reach the bone (usually medullar one) through hematogenous route or by direct inoculation (trauma) developing an acute infection with polymorphonuclear infiltrates, cytokines and an inflammatory reaction. Then, a cavity (*sequestrum*) is provoked, where the bacteria form a *biofilm* inside the bone. This *biofilm* involves a bacterial community embedded within a dense and protective extracellular matrix,

which constitutes a primary barrier in its treating. Thus, bacteria within the *biofilm* can evade both the host immunological response and the action of antimicrobial agents [5–7]. OM treatment remains a significant clinical challenge due to the disadvantages presented by current therapies. Such therapies involve systemic antibiotics administration and surgery, with serious repercussions for the patients as high incidence of side effects, prolonged hospital stays, and even, high morbidity rate [8–11].

Recently, the scientific efforts are directed to the design of 3D scaffolding that dynamically contribute to the regeneration process, promoting integration, osteoconduction and angiogenesis, avoiding bacterial infection and/or offering many other desired functions to promote faster and secure healing [12–17]. Despite all the advancements, there are still challenges to be addressed in the field of local bone drug delivery including effective and sustained release control, prolonged drug stability and activity as well as the cell toxicity [18,19]. Ideally, the local release from 3D scaffolds should preserve the stability of the loaded active molecules over time and ensure a precise control over the drug release rate [20]. This fact can be

\* Corresponding authors at: Departamento de Química Inorgánica y Bioinorgánica, Facultad de Farmacia, Universidad Complutense de Madrid, Instituto de Investigación Sanitaria Hospital 12 de Octubre i+12, Plaza Ramón y Cajal s/n, 28040 Madrid, Spain.

Email addresses: ibarba@ucm.es (I. Izquierdo-Barba); vallet@ucm.es (M. Vallet-Regí)

understood as a way of smart drug delivery. In this sense, pH responsive approaches can allow a selective release approach either through changing the solubility of the drug carrier or through cleaving of pH responsive bonds upon variation of microenvironment pH [21,22]. Such pH variations, from physiological pH (7.4) to pH values between 6.7 and 5.5, are due to the production of metabolites as lactic acid by the microorganism proliferation [23,24]. However, these pH responsive devices, in the most of the cases do not response to these variations, detecting more abrupt pH changes [25].

Recently, hierarchical meso-macroporous 3D scaffolds based on *nanocomposite* formed by nanocrystalline apatite uniformly embedded into a mesostructured  $\text{SiO}_2\text{-CaO-P}_2\text{O}_5$  glass wall (MGHA) have been fabricated by rapid prototyping technique [26–28]. These MGHA 3D scaffolds have shown excellent properties as highly bioactive behavior, enhanced biocompatibility, no induction of inflammatory response, as well as good preosteoblast adhesion, colonization, proliferation and differentiation (see supporting information Fig. S1). Unlike other reported 3D systems [12–17,29,30], these MGHA 3D scaffolds are made up exclusively of pure ceramic nanostructured material and not ceramic-polymer combinations, which exhibit excellent bioactivity together with greater homogeneity of these platforms. All these characteristics suggest their great potential application as multifunctional 3D biomaterials for both bone tissue engineering and local drug delivery systems.

Herein, with the aim of using these MGHA 3D scaffolds for treatment and prevention of OM, they have been loaded with levofloxacin (Levo). This quinolone antibiotic has been chosen because: (i) it is a broad spectrum antibiotic used in bone infection therapy, which penetrates into both trabecular and cortical bone, (ii) it minimizes the risk of bacteria resistance and (iii) it exhibits different protonation states (cationic, *zwitterionic*, and anionic states) as a function of pH, which could lead to different interactions between Levo and silanol groups of the mesoporous matrix [31–33]. Thus, this work is focused on the design of multifunctional MGHA 3D scaffolds with the ability of pH-releasing Levo to inhibit the *S. aureus* growth and to destroy the *biofilm*, and at the same time allowing an adequate osteoblast colonization. For these purposes, *in vitro* Levo release has been performed at different pHs to confirm the pH-dependent release. The effectiveness of these 3D hierarchical systems has been evaluated by both *in vitro* bacterium/bone cell co-culture model and on preformed Gram-positive bacterial *biofilms*. Finally, the possible cytotoxic effects induced by the highest Levo dose released from MGHA 3D scaffolds were evaluated with cultured human Saos-2 osteoblasts. In the present study, MGHA 3D-Levo scaffolds have been designed with two objectives: i) to prevent bacterial contamination after placing the scaffold in a bone defect to act as a template for tissue formation and ii) to treat bone defects caused by infection (osteomyelitis).

## 2. Materials and methods

### 2.1. Preparation and characterization of MGHA scaffolds

MGHA 3D scaffolds based on *nanocomposite* material were prepared by rapid prototyping (RP) using methylcellulose (MC), as previously reported [27,28]. These 3D scaffolds have been characterized by X-ray diffraction (XRD) in a Philips X'Pert diffractometer (Eindhoven, The Netherlands), equipped with  $\text{Cu K}\alpha$  (40 kV, 20 mA). The textural properties were determined by  $\text{N}_2$  adsorption porosimetry using a Micromeritics ASAP2020 analyzer (Norcross, USA). The surface area ( $S_{\text{BET}}$ ) was determined using the multipoint Brunauer-Emmett-Teller method included in the software. The total pore volume ( $V_p$ ) was calculated from the amount of  $\text{N}_2$  adsorbed at a relative

pressure of 0.97. The average mesopore diameter ( $D_p$ ) was obtained from the adsorption branch of the isotherm by means of the Barrett-Joyner-Halenda (BJH) method [34]. Morphological structure analysis was performed by scanning electron microscopy (SEM) using a field emission JEOL JSM 6335F microscope (Tokyo, Japan) at an acceleration voltage of 10 kV. The nanostructure was characterized by Transmission electron microscopy (TEM) was performed on a JEOL 3010 electron microscope (Jeol Ltd., Japan) operating at 300 kV (Cs; 0.6 mm, resolution 1.7 °Å). The porosity was measured by Hg intrusion porosimetry in a Micromeritics Autopore IV 9500 device (Micromeritics Instrument Corporation, Norcross, GA, USA). Elemental analyses (C, H, N) were carried out on a LECO CHNS-932 micro-analyzer (Saint Joseph, Michigan, USA). Fourier Transform Infrared (FTIR) spectroscopy was performed in a Thermo Nicolet Nexus spectrometer (Thermo Scientific, USA) from 4000 to  $400\text{ cm}^{-1}$ , using the KBr pellet method and operating in transmittance mode.

### 2.2. Levofloxacin loading into MGHA scaffolds

Levo incorporation into the MGHA 3D scaffolds was carried out by the impregnation method [35]. For this propose, the 3D scaffolds were soaking individually (with a mass of  $23 \pm 2\text{ mg}$ ) in 3 mL of an Levo ethanolic solution [ $3.7\text{ mg/mL}$ ], at room temperature (RT), as previous results in powder [35]. After 24 h in orbital shaking at 200 rpm, they were removed, vigorous washed with pure ethanol and dried at RT. The handling of these scaffolds was performed in the dark conditions due to its sensitivity to light. The amount of drug incorporated was determined by elemental chemical analysis. Each load measurement was performed in quadruplicate. The 3D scaffolds loaded with Levo have been named as MGHA 3D-Levo scaffolds.

### 2.3. Levofloxacin release from MGHA 3D-Levo scaffolds

The release kinetic studies of Levo were carried out in phosphate buffered saline (PBS) solution at different pHs: 5.5, 6.7 and 7.4, to study the pH influence on the release kinetic. In these studies, each MGHA 3D-Levo scaffolds (supported vertically with a Pt wire) has been soaked in 15 mL of PBS, with the pH adjusted previously, at 37 °C and orbital shaking at 300 rpm. The media have been removed daily. The Levo released has been quantified using a spectrofluorimeter Biotek Power wave XS, version 1.00.14 of the Gen5 program, with a  $\lambda_{\text{excitation}} = 292\text{ nm}$  and  $\lambda_{\text{emission}} = 494\text{ nm}$  [33]. Different calibration lines have been calculated at different pHs in a concentration range of 12–0.01  $\mu\text{g/mL}$ .

### 2.4. Antimicrobial activity of the MGHA-Levo scaffolds

Prior to the all *in vitro* tests, the samples were sterilized by UV light radiation during 10 min in both sides. Then the samples were immersed in 6 mL of PBS under a 5%  $\text{CO}_2$  atmosphere at 37 °C for 1 h to become stabilized and eliminate some residual agents before the *in vitro* culture. The efficacy against bacterial growth and *biofilm* has been determined using the *S. aureus* 15981 laboratory strain, due to the most of the bone infections are caused by this kind of bacteria [16]. Briefly, bacteria were inoculated in tryptic soy broth (TSB; Bio-Merieux, Marcy L'Etoile, France) and incubated overnight at 37 °C with orbital shaking at 200 rpm. After culture, bacteria were centrifuged for 10 min at 3500g at 22 °C. The supernatant was then discarded and the pellet was washed three times with sterile PBS. The bacteria were then suspended and diluted in PBS to obtain a concentration of  $10^8$  colony forming units (CFU) per mL; the bacterial concentration was determined by spectrophotometry using a visible spectrophotometer (Photoanalyzer D-105, Dinko instruments). To deter-

mine their effectiveness over time against *S. aureus* growth, 3D scaffolds were soaked in 2 mL of PBS containing bacteria at  $10^8$  CFU/mL of concentration. This solution was removed daily during a period of time of 1 to 15 days. The presence or not of bacteria, as well as their quantification, was determined on the PBS solution in contact with the MGHA 3D-Levo scaffolds. The determination of bacteria amount was performed by CFU in agar. In this sense, 10  $\mu$ L of this solution was seeded onto TH agar and incubated at 37°C overnight and posterior count. The minimum inhibitory concentration (MIC) of Levo has been also calculated, obtaining a value of 0.06  $\mu$ g/mL for these experiments. Moreover, a direct observation of MGHA 3D-Levo scaffold surfaces was also performed by confocal microscope in a Biorad MC1025 microscope. For these experiments, the samples were stained for 15 min with a Live/Dead® Bacterial Viability Kit (Backlight™). Staining was performed with a mixture of dyes: SYTO 9 (live bacteria/green) and propidium iodide (dead bacteria/red). SYTO 9 fluorescence was excited at 480/500 nm, and the emitted fluorescence measured at 500 nm, and propidium iodide fluorescence was excited at 490/635 nm, with the emitted fluorescence measured at 618 nm [36]. Controls with MGHA 3D scaffolds without Levo were always carried out in all the experiments.

Moreover, the effectiveness of these MGHA 3D-Levo scaffolds against *biofilm*, previously formed onto cover glass disks, was also determined. For these purposes, *S. aureus* *biofilms* were previously developed by suspended cover glass disks in a bacteria solution of  $10^8$  bacteria per mL during 48 h at 37°C and orbital stirring at 100 rpm. In this case, the medium used was 66% TSB+0.2% glucose to promote robust *biofilm* formation. After that, the cover glass disks containing bacterial *biofilm* were localized onto six well culture plates (CULTEK) in 6 mL of new medium. Then, MGHA 3D-Levo scaffolds were submerged avoiding the direct contact with *biofilm* coated glass disk. After 24 h of incubation, the glass-disk were washed three times with sterile PBS, stained with a 3  $\mu$ L/mL of Live/Dead® Bacterial Viability Kit (Backlight™) and 5  $\mu$ L/mL of calcofluor solution to specifically determine the *biofilm* formation, staining the mucopolysaccharides layer (extracellular matrix in blue). Both reactants were incubated for 15 min at RT. *Biofilm* formation was examined in an Olympus FV1200 confocal microscope [36].

## 2.5. *In vitro* co-culture studies. MC3T3-E1 preosteoblasts vs *Staphylococcus aureus*

Since multifunctional 3D systems involve both antibiotic release and bone regeneration processes, the need for a flexible *in vitro* test system highly representative of *in vivo* conditions is of paramount importance before carrying out any tests on animals. Such model system allows more realistic assessment of different clinical treatment options in a rapid, cost-efficient, and safe manner, especially regarding to test possibly host-toxic therapies [37,38]. Here, we have established an *in vitro* bacterium/bone cell co-culture model system to evaluate these 3D systems for the prevention and treatment of OM. A preliminary, co-culture assays was carried out by seeding MC3T3-E1 cells (a murine calvaria-derived pre-osteoblastic cell line used as an archetypal model of *in vitro* osteogenesis [39,40]) and *S. aureus* 15981 laboratory strain on the 3D-scaffolds (MGHA and MGHA Levo scaffolds), concurrently performing the corresponding control studies of osteoblasts and bacteria individually. First of all, the preosteoblastic cells were grown in complete Dulbecco's Modified Eagle's Medium ( $\alpha$ -DMEM, Sigma Chemical Company, St. Louis, MO, USA) supplemented with 2 mM L-glutamine (BioWhittaker), 100  $\mu$ g mL<sup>-1</sup> penicillin (BioWhittaker), 100 g mL<sup>-1</sup> streptomycin (BioWhittaker) and fetal bovine serum (FBS, Gibco) at 10% at 37°C

under atmosphere conditions of 95% humidity and 5% CO<sub>2</sub>. Medium was changed every day until confluence reached  $\approx$ 90%. Cells were washed with PBS, harvested using 0.25% trypsin-EDTA solution (Sigma Aldrich), counted with a Neubauer Hemocytometer and collected. Cells were then centrifuged at 310g for 10 min and suspended in fresh medium without antibiotics at a density of  $2 \cdot 10^4$  cells/mL. Simultaneously, *S. aureus* bacteria were cultured in the same conditions and taken at a density of  $2 \times 10^8$  cells/mL, mimicking an infectious process. Then 500  $\mu$ L of both preosteoblast and bacteria suspensions were seeded onto 3D scaffolds and incubated different times at 37°C under atmosphere conditions of 95% humidity and 5% CO<sub>2</sub>. Then, the samples were washed twice with sterile PBS and fixed with paraformaldehyde (Sigma Aldrich) 4%+1% (w/v) sucrose (Sigma Aldrich) in PBS for 40 min. Afterwards, samples were again washed with PBS and permeabilized with 0.5% Triton X-100 (Sigma Aldrich) at 4°C for 5 min. Nonspecific union sites were blocked with 1% (w/v) bovine serum albumin (BSA) (Sigma Aldrich) incubated at 37°C for 20 min. Finally, samples were stained with Atto 565 conjugated with phalloidin (ratio 1:40, Sigma Aldrich) for cytoplasm  $\alpha$ -F-actin filaments dying and then stained 2 min with 100  $\mu$ L of DAPI (Thermo Fisher Scientific) for eukaryotic nuclei visualization and bacteria. Finally, the samples were washed with PBS and maintained in PBS for confocal analysis. Moreover, lactate dehydrogenase activity (LDH) was determined in the culture medium in contact with the 3D scaffolds after 6, 24 h and 3 days of incubation to evaluate the plasma membrane integrity. Activity of LDH released by the MC3T3-E1 cells is directly related to the rupture of the plasma membrane that produces the release of enzymes present in the cytoplasm. Measurements were performed by using a commercial kit (Spinreact) at 340 nm with a Beckman DU 640 UV-Visible spectrophotometer Unicam UV-500 and calculated in terms of absorbance variation by minute to obtain the units per litre concentration ( $\Delta A/\text{min } 4925 = \text{U/L LDH}$ ).

## 2.6. Culture cell for the *in vitro* biocompatibility studies

The *in vitro* biocompatibility assays were carried out on human osteosarcoma Saos-2 cell line, which is usually used as experimental model in this kind of *in vitro* studies due to its osteoblastic properties as production of mineralized matrix, high alkaline phosphatase levels, PTH receptors and osteonectin presence [41]. Human Saos-2 osteoblasts (purchased from American Type Culture Collection, ATCC) were seeded on six well culture plates (CULTEK), at a density of  $10^5$  cell/mL in DMEM supplemented with 10% fetal bovine serum (FBS, Gibco), 1 mM L-glutamine (BioWhittaker), penicillin (200  $\mu$ g/mL, BioWhittaker), and streptomycin (200  $\mu$ g/mL, BioWhittaker), under a CO<sub>2</sub> (5%) atmosphere and at 37°C for 24 h. MGHA and MGHA-Levo scaffolds were soaked in 15 mL of DMEM at 37°C and orbital shaking at 200 rpm, obtaining the supernatants with the Levo dose released after 3 and 24 h. Controls of DMEM without scaffolds were also prepared. All these media were added to cultured human Saos-2 osteoblasts and cells were incubated for 24 h. Then, cells were washed with PBS, harvested using 0.25% trypsin-EDTA solution, and counted with a Neubauer hemocytometer for the analysis of cell proliferation. Cells were then centrifuged at 310g for 10 min and resuspended in fresh medium for the analysis of viability, cell cycle, apoptosis, intracellular reactive oxygen species (ROS) content, cell size, and complexity by flow cytometry as described below.

### 2.6.1 Flow cytometry studies

After incubation with the different probes, the conditions for the data acquisition and analysis were established using negative and

positive controls with the CellQuest Program of Becton Dickinson. For statistical significance, at least 10,000 cells were analyzed in each sample.

### 2.6.2 Cell viability and intracellular ROS content

After detachment of Saos-2 osteoblasts, cell suspensions were incubated with 100  $\mu\text{M}$  2',7'-dichlorofluorescein diacetate (DCFH/DA) at 37°C for 30 min. DCF fluorescence was excited at 488 nm and measured with a 530/30 nm band pass filter in a FACScalibur Becton Dickinson flow cytometer. Cell viability was determined by addition of propidium iodide (PI; 0.005% in PBS) to stain the DNA of dead cells. The fluorescence of PI was excited at 488 nm, and the emission was measured with a 670 nm LP in the cytometer described above.

### 2.6.3 Cell cycle analysis and apoptosis detection

Cell suspensions were incubated with Hoechst 33258 (Poly Sciences, Hoechst 5  $\mu\text{g/mL}$ , ethanol 30%, and BSA 1% in PBS), used as a nucleic acid stain, for 30 min at RT in darkness. The Hoechst fluorescence was excited at 350 nm, and the emission was measured at 450 nm in a LSR Becton Dickinson flow cytometer. The cell percentage in each cycle phase:  $G_0/G_1$ , S, and  $G_2/M$  was calculated with the CellQuest Program of Becton Dickinson, and the SubG1 fraction (cells with fragmented DNA) was used as indicative of apoptosis.

### 2.6.4 Cell size and complexity

After detachment of Saos-2 osteoblasts, forward angle (FSC) and side angle (SSC) scatters were evaluated as indicative of cell size and complexity respectively using a FACScalibur Becton Dickinson flow cytometer.

## 2.7. Statistics

All data are expressed as means  $\pm$  standard deviations of a representative of three experiments carried out in triplicate. Statistical analysis was performed using the Statistical Package for the Social Sciences (SPSS) version 19 software. Statistical comparisons were made by analysis of variance (ANOVA). Scheffé test was used for post hoc evaluations of differences among groups. In all of the statistical evaluations,  $p < .05$  was considered as statistically significant.

## 3. Results and discussion

### 3.1. Characterization of the MGHA 3D-Levo scaffolds

A deep morphological and structural characterization of MGHA 3D-Levo scaffolds was carried out with different techniques and is summarized in Fig. 1. By different SEM microscopies, a high and regular level of hierarchical porosity from macro to mesoporous ranges are shown. In this sense, different scales of porosity can be observed: (i) ultra-large macropores of ca. 450  $\mu\text{m}$ ; (ii) macropores with diameters of ca. 80  $\mu\text{m}$  interconnected and (iii) highly ordered mesopores in 2D hexagonal ( $p6mm$ , plain group) structure with diameters of ca. 9 nm. These results evidence the hierarchical structure of MGHA 3D-Levo scaffolds. A study by mercury intrusion porosimetry was carried out, confirming also that the Levo impregnation process does not affected to the macroporous properties of these scaffolds (data not shown). To confirm qualitatively the presence of Levo, MGHA 3D-Levo scaffolds were characterized by FTIR (Fig. 1, bottom). We can observe characteristic bands of Levo molecule (which are indicated by arrows) to 3265  $\text{cm}^{-1}$  due to carboxylic

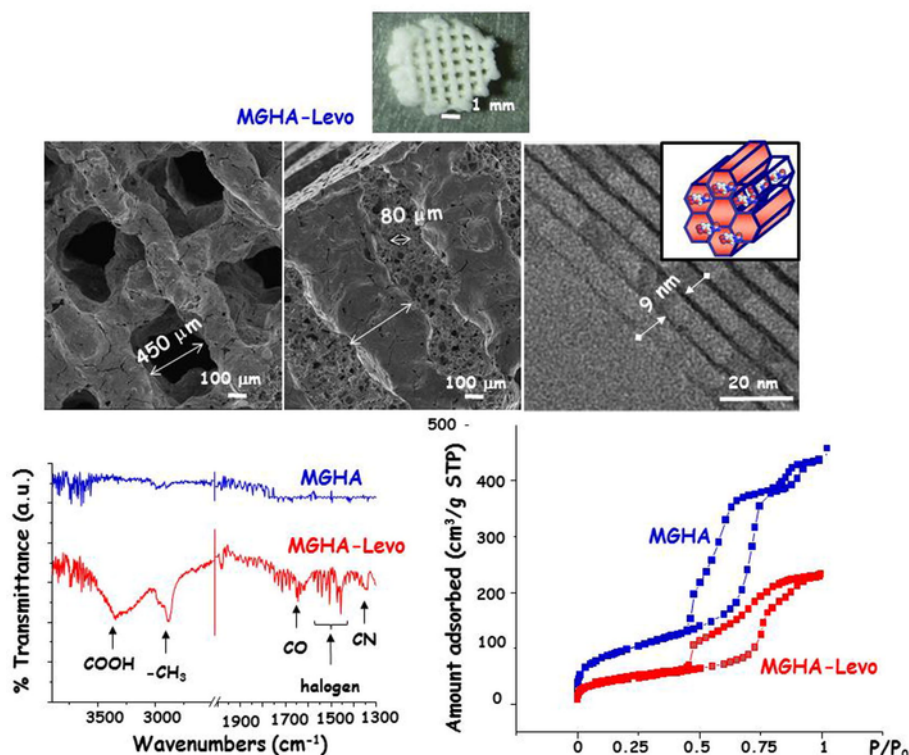


**Fig. 1.** Characterization of 3D MGHA scaffolds before and after Levo loading. (Top) Morphological and structural characterization by SEM and TEM showing a high a regular level of hierarchical porosity from macro to mesoporous. (Bottom) FTIR spectra and  $\text{N}_2$  adsorption isotherms of 3D MGHA scaffolds before and after drug loading confirming the presence of Levo and an decrease of textural properties in the mesoporous range.

group,  $2931\text{ cm}^{-1}$  due to alkanes group stretching,  $1724\text{ cm}^{-1}$  due to stretching of carbonyl group,  $1294\text{ cm}^{-1}$  due to stretching of amines, between  $1100$  to and  $1400\text{ cm}^{-1}$  due to the presence of halogen group. Once confirmed the presence of drug, a study by elemental chemical analysis was carried out to calculate the amount of antibiotic loaded by each scaffold. Moreover, the textural properties of these 3D scaffolds were analyzed by  $\text{N}_2$  adsorption porosimetry with the purpose to determine the incorporation of Levo into their mesoporous structure. Table 1 shows the percentage (%) of Levo in each MGHA 3D-Levo scaffolds and the variation of their textural properties before and after impregnation process. Concerning to the yielding of the loading process, MGHA 3D-Levo scaffolds loaded a 3% of Levo respect to the total drug concentration used in the impregnation solution. Although a priori, this percentage would seem low, it is within the normal range of loading of a drug by the impregnation method [42].  $\text{N}_2$  adsorption studies (Fig. 1 and Table 1) show a significant decrease in the textural properties, from values of  $123\text{ m}^2/\text{g}$  and  $0.2\text{ cm}^3/\text{g}$  for specific surface area and total pore volume, respectively, to  $40\text{ m}^2/\text{g}$  and  $0.1\text{ cm}^3/\text{g}$  before and after drug loading. Also, a slight variation in pore diameter was observed, exhibiting a value of

$9.3\text{ nm}$  in the MGHA-Levo scaffolds versus  $10\text{ nm}$  in the MGHA scaffolds without Levo. It is known that the decrease in the values of specific surface area, total pore volume and pore diameter after drug loading process is related to the confinement of the drug into the mesoporous structure according with the literature [42].

Finally, to determine if the impregnation process affects to mesoporous arrangement and crystallinity of both apatite phase of MGHA scaffolds and the drug, XRD studies have been carried out. Fig. S2 shows XRD patterns at low and wide scattering angles corresponding to a MGHA 3D-Levo scaffolds. Low angle XRD pattern (left) shows a well-defined diffraction maximum at  $2\theta=0.86$  degree and wide maxima around  $2\theta=1.43$  and  $1.67$  degree, which can be indexed as 10, 11 and 20 reflections of a 2D-hexagonal structure with  $p6mm$  plane group. Wide angle XRD pattern (right) reveals the presence of nanocrystalline apatite phase exhibiting (002), (211) and (310) reflections. These results highlight that Levo incorporation into the mesoporous structure does not affect their mesostructural order, maintaining the 2D-hexagonal structure and the crystallinity of the apatite phase of the pore wall. Moreover, Levo does not crystallize into mesoporous network, as it has been also shown for other mesoporous matrices and other drugs [43].

### 3.2. *In vitro* levofloxacin release kinetics

The *in vitro* drug release assays from MGHA 3D-Levo scaffolds were carried out at different pH values in PBS to determine the pH-dependent Levo release. Thus, pH 5.5 and pH 6.7 were used as representative values of an infectious process, and pH 7.4 as value in physiological conditions [23,25]. Fig. 2 displays *in vitro* release profiles, which are expressed as accumulative drug release as function of the time. The obtained results show significantly higher release at acid pH values (pH 5.5 and 6.7) than that obtained at physiological conditions (pH 7.4), which follows a slow and sustained drug release. In

**Table 1**

Levo loaded (%) into the mesoporous structure of MGHA-Levo scaffolds. Textural properties: BET surface area ( $S_{\text{BET}}$ ), pore volume ( $V_p$ ) and pore diameter ( $D_p$ ) before and after the impregnation process.

Samples	% Levo	$S_{\text{BET}}$ ( $\text{m}^2/\text{g}$ )	$V_p$ ( $\text{cm}^3/\text{g}$ )	$D_p$ (nm)
MGHA	—	123	0.2	10.0
MGHA-Levo	3	40	0.1	9.3

$S_{\text{BET}}$  is the specific surface area determined by the BET method.  $V_p$  is the total pore volume calculated using the single point method at  $P/P_0=0.99$ .  $D_p$  is the pore diameter calculated from the analysis of the adsorption branch of the isotherm using the BJH method.

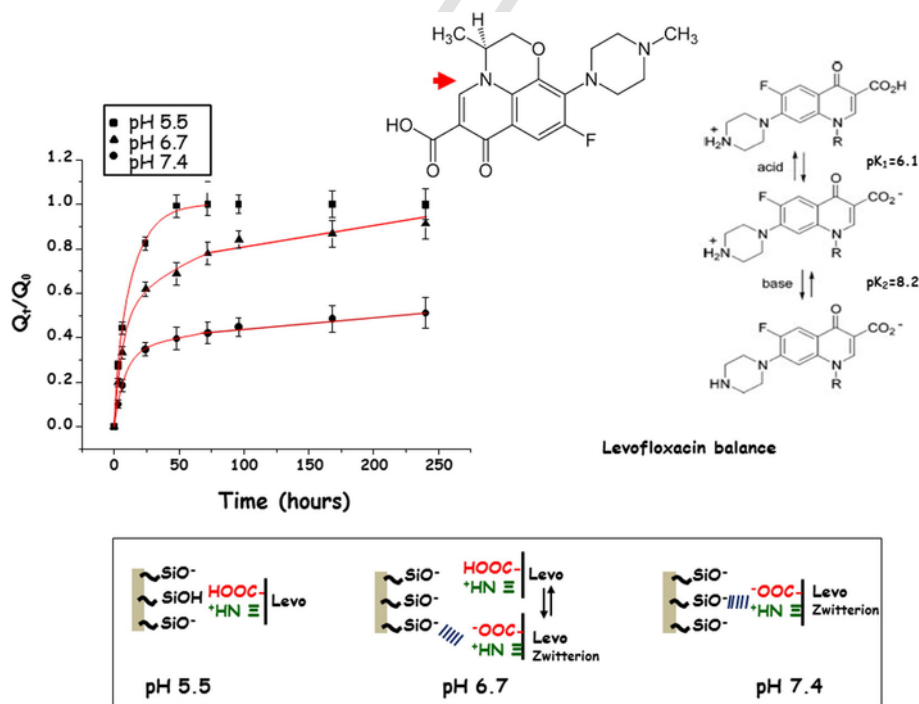


**Fig. 2.** pH-dependent Levo release from MGHA-Levo scaffolds. (Left) *In vitro* release profiles to pH 5.5, pH 6.7 and pH 7.4. The curves represent the cumulative amount of Levo released ( $Q_t$ ) with respect to the amount of Levo initially present in the scaffold ( $Q_0$ ) versus time. (Right) Levo acid-basic balance at different pHs. (Bottom) Scheme showing the possible interactions between the silanol groups of the mesoporous matrix and the Levo ionizable groups to different pHs.



general, the drug release kinetics from mesoporous matrices are governed, primarily by drug diffusion processes throughout the matrix. Such drug diffusion processes are fitted, generally, to the Higuchi model. However, our results suggest that in addition to the drug diffusion process throughout the mesoporous matrix, a new component is governing the drug release kinetics. Specifically, this new component refers to the MGHA matrix-Levo interactions, as it has been previously reported for other silica matrix [44,45].

Fig. 2 shows a schematic representation of the different interactions between silanol (Si-OH) groups of 3D scaffolds and Levo ionizable groups. Levo molecule exhibit an isoelectric point of 7.1 with different pH-dependent protonation states *i.e.* cationic, *zwitterionic*, and anionic forms. These different protonation states are due to the presence of 6-carboxylic acid and the N4 piperazinyl group in the Levo molecule, with pKa values of 6.1 and 8.2, respectively. Concerning to the MGHA matrix, SiOH groups have a pKa value of 4.5. Thus, at pH 5.5, the 3D scaffolds surface exhibits deprotonated (SiO<sup>-</sup>) negatively charged and Levo molecule, is in cationic form, resulting fast release as it is observed in the release kinetics. This situation changes slightly at pH 6.7, where the most of the Si-OH groups are deprotonated and Levo is in two different protonation states, *i.e.*, in cationic form and as *zwitterion*, coexisting both species. *Zwitterionic* species have the ability to form hydrogen bonds with silanol matrix, leading to a slower release at this pH as it has been reported elsewhere [33]. Finally, at pH 7.4, the most Levo molecules are in *zwitterionic* form, which favors the formation of more hydrogen bonds, showing a slow and sustained release, based on the high stability of the hydrogen bonds compared to other electrostatic interactions [33].

These studies reveal that Levo release from MGHA 3D-Levo scaffolds is pH-dependent, since drug-carrier interaction and subsequent release can be modulated by pH changes. Specifically, drug release increases as decreasing pH. Also, the drug-carrier interaction is reversible, allowing Levo to be released in a sustained and/or controlled manner. Thus, to confirm this hypotheses, the theoretical kinetic model adopted in this work considers first-order diffusion/convection ( $k_s$ ) and drug association/dissociation ( $k_{off}$ ) following the Eq. (1) [45]. This model leads to a decoupling of drug association/dissociation with its diffusion/convection: fast release of initially free drug molecules via diffusion/convection and slow release of bound drug molecules, that is dictated by the dissociation process.

$$\frac{Q_t}{Q_0} = \frac{k_{off}}{k_{on} + k_{off}} (1 - e^{-k_s t}) + \frac{k_{on}}{k_{on} + k_{off}} (1 - e^{-k_{off} t}) \quad (1)$$

where  $Q_t/Q_0$  correspond to accumulative amount of drug released with respect to the amount of drug initially presents in the matrix, per unit time.  $k_s$  is the diffusion constant and,  $k_{off}$  and  $k_{on}$  correspond to dissociation/association constants, respectively. The drug that does not interact with the matrix is governed mainly by  $k_s$ , whereas that the drug-matrix interaction is governed by  $k_{off}$ . In this model, the free energy difference ( $\Delta G$ ) between drug free and drug bound to the matrix can also be calculated. This parameter determines the initial burst effect and, it is expressed in the Eq. (2).

$$\Delta G = -k_B T \ln \left( \frac{k_{on}}{k_{off}} \right) \quad (2)$$

where  $k_B$  is the Boltzmann constant and,  $T$  is the system absolute Temperature in Kelvin grades. Fitting experimental release patterns to Eq. (1) allowed the determination of the experimental values for

$k_s$ ,  $k_{on}$  and  $k_{off}$ . Then,  $\Delta G$  was calculated from Eq. (2). The experimental results are summarized in Table 2. The obtained results show a notable increase in  $k_s$ ,  $k_{off}$  and  $\Delta G$  parameters, by decrease of pH.

At pH 7.4, the  $k_{off}$  value is very low, which means that most of the drug interacts with the matrix, having a small amount of drug dissociated and therefore, low  $k_s$  and  $\Delta G$ . On the contrary, at pH 6.7, the drug-matrix unions start to dissociate as consequence of changes in the Levo protonation states. It results in an increase of the  $k_s$  and  $k_{off}$  constants and of the  $\Delta G$  parameter. Finally, the more significant increase, is at pH 5.5. In this case, no Levo-matrix interactions are possible, obtaining the higher amount of Levo released. The obtained results confirm that the release profiles can be fitted to a kinetic model, which combines two parameters, *i.e.* reversible interaction matrix drug as function of pH and drug diffusion process throughout the matrix. These pH dependent release are promising since nowadays, one of the main risks of the drug sustained release over time is the appearance of antibiotic-multiresistant strains [19,45,46]. Fortunately, the higher amount of Levo released from MGHA scaffolds is produced as the pH decreases, and it only occurs when there is a high bacterial proliferation. Therefore, the pH-dependent Levo release from our systems could minimize the risk of antibiotic resistant strains [46].

### 3.3. In vitro antimicrobial activity

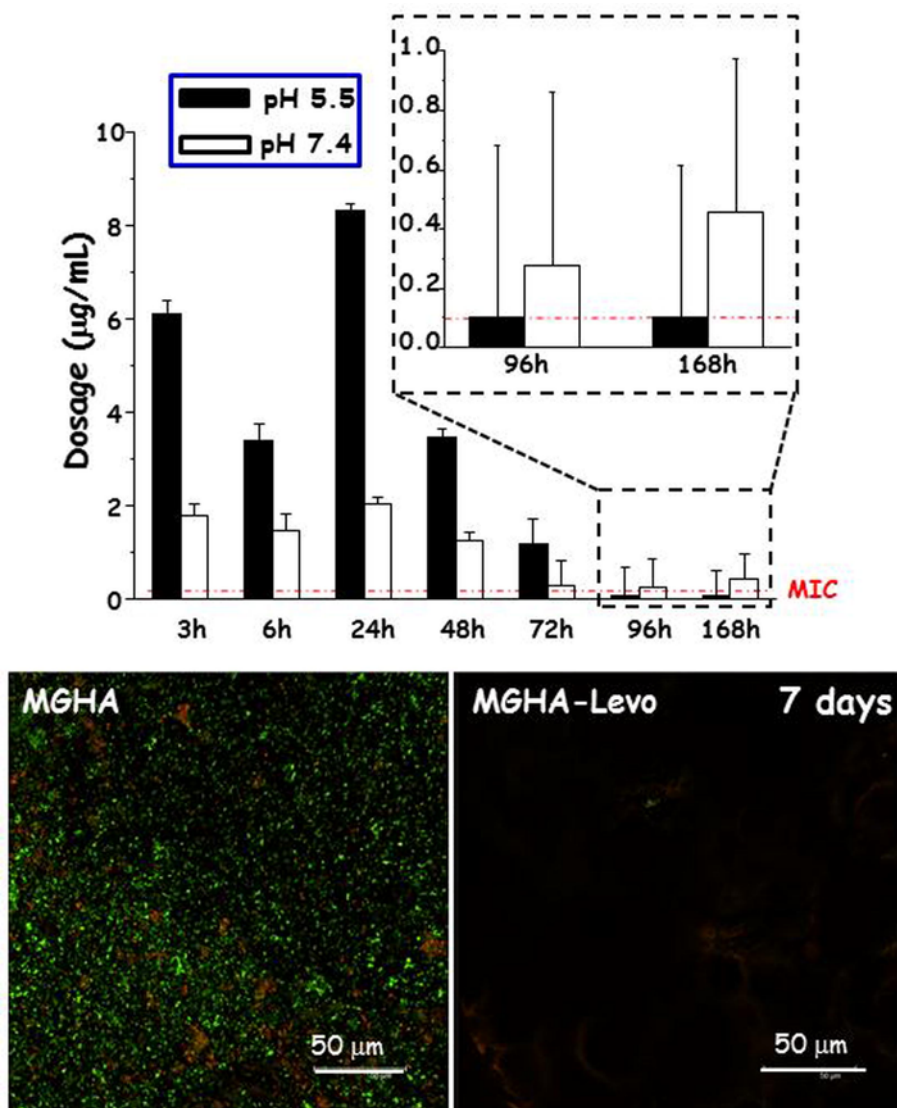
The 3D MGHA-Levo scaffolds microbiological effectiveness was determined studying the *S. aureus* growth inhibition. Fig. 3 displays Levo dose daily released at pH 7.4 and pH 5.5 and its microbiological activity against this strain after 7 days of incubation. The MIC in these conditions was of 0.06 µg/mL, which is according to the MIC values for *S. aureus*, obtaining by other authors [46]. The results evidence a Levo daily dose higher than the MIC, during 7 days of incubation. After this time, colony forming unit (CFU) of this bacterial strain grew in the agar plates, confirming loss of antimicrobial activity (data not shown). A local antibiotic administration system provides therapeutic benefits when it ensure a drug concentration adequate in the tissue. This requires that the drug dose daily released is several times higher than the MIC of the microorganism causing the infection [46]. Levo dose (µg/mL) daily released from MGHA-Levo scaffolds is, during 7 days, higher than the MIC for the bacterial strain studied, thus, this system could be effective to prevent an implant-associated infection. A direct assay by confocal microscopy has been carried out for demonstrating the microbiological effectiveness of the MGHA-Levo scaffolds. Fig. 3 (bottom) details comparatively the MGHA scaffolds surface without Levo (left) and MGHA-Levo scaffolds (right) after 7 days of incubation with a *S. aureus* concentration [ $10^8$  bacteria/mL] daily renewed. Results show the MGHA scaffolds surface without Levo completely covered of mantle of *S. aureus*. By the contract, the MGHA-Levo scaffolds surface shows total absence of bacteria demonstrating their effectiveness after 7 days of incubation.

Fig. 4 summarizes the obtained results to determine the effectiveness of Levo containing 3D MGHA scaffolds against *S. aureus*

**Table 2**

Kinetic parameters estimated in the Eq. (1). The parameters  $K_{off}(h^{-1})$ ,  $K_s(h^{-1})$ ,  $\Delta G(10^{-21}J)$  and  $R^2$  correspond to drug-matrix dissociation/association constants, the free energy difference and the correlation coefficient, respectively.

pH	$K_{off}(h^{-1})$	$K_s(h^{-1})$	$\Delta G(10^{-21}J)$	$R^2$
7.4	0.002	0.121	2.71	0.997
6.7	0.011	0.155	4.19	0.996
5.5	0.067	0.435	19.15	0.999



**Fig. 3.** Levo dose profile daily released. (Top) Levo dose (µg/mL) released over time to pH 5.5 and pH 7.4. The antimicrobial activity against *S. aureus* has been evaluated in the range of 30–0.02 µg/mL, obtaining a value of MIC of 0.06 µg/mL. \* [ $10^8$  bacteria/mL] daily renewed. (Bottom) A representative image of confocal microscopy.

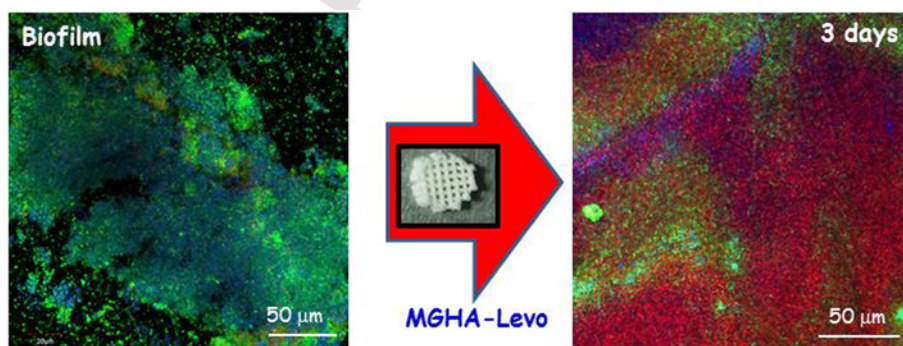


**Fig. 4.** *In vitro* antimicrobial activity against *S. aureus* biofilm of MGHA-Levo scaffold by confocal microscopy. (Left) Preformed *S. aureus* biofilm stained by SYTO (Green, alive bacteria) and Calcofluor (blue, mucopolysaccharide covered). (Right) scenario after 3 days with 3D scaffolds treatment containing Levo showing almost the bacteria stained with IP (red, dead bacteria).

*biofilm*, showing almost the total *biofilm* destruction after 3 days of incubation. Before treatment (left image), the confocal image shows the *biofilm* surface formed by lived bacteria (green) covered with mucopolysaccharide coating (blue). After 3 days of treatment, the scenario is significant different showing almost the total of bacteria dead (red), demonstrating the effectiveness of these 3Dscaffolds against gram-positive *biofilm* bacteria.

It has been demonstrated that most cases of osteomyelitis are caused by *S. aureus*, however they can coexist with other bacteria types with different etiology as *S. epidermidis* [5,19,24]. Moreover, pathogenic characteristics of collection organisms are different to that from clinical isolates (which can have up to 20% more genes [47]). Therefore, although the results obtained in this study are promising, it is important to remark that it is only a preliminary assay that need further *in vitro* research (and obviously *in vivo* one) before considering these results orientative for all important etiologies.

### 3.4. *In vitro* MC3T3-E1 preosteoblast and *S. aureus* co-culture assays

To evaluate the multifunctional capability concerning to both antimicrobial activity and bone regeneration in an OM scenario, *in vitro* MC3T3-E1/*S. aureus* co-culture assays were carried out. For this purpose, MC3T3-E1 osteoblast-like cells and *S. aureus* were seeded on both MGHA and MGHA-Levo 3D scaffold surfaces. The concentrations used were of  $10^8$  cfu/mL *S. aureus* (suspended in TSB) and  $10^4$  MC3T3-E1 osteoblast-like cells/mL (suspended completed medium DMEM). Fig. 5 provides two series of images (MGHA and MGHA-Levo 3D scaffolds) of the time progress followed in co-culture assays highlighting the expected effects of the material in each case. In the case of MGHA scaffolds without Levo, at longer times (24h), apoptotic cells appear as rounded red spots while the *biofilm*

maturation keeps in successful progress until a fully developed state with osteoblast complete disruption and disappearance. In the case of co-cultures on MGHA-Levo scaffold, the outcomes are much more inspiring than before. The confocal images after 6h show the absolute absence of bacterial population adhered to the material surface and osteoblasts healthily attached and growing. Finally, posterior time images after 24h and 3 days demonstrate the scaffold surface clean of bacteria with an adequate cell colonization, evidencing again a great biocompatibility, as it has also been demonstrated for others 3D systems with co-administration of vancomycin and BMP-2 on *in vitro* co-culture [38].

On the other hand, lactate dehydrogenase (LDH) test was performed to (i) assess the cytotoxicity caused by the biomaterial itself (MGHA and MGHA-Levo 3D scaffolds) and (ii) evaluate the status of preosteoblasts under the co-culture conditions. These results (data not shown) show a significant increased LDH released in MGHA scaffold co-culture conditions, which increases with time. This is due to the co-existence of cells and bacteria, as the later ones have a cytotoxic effect on the osteoblasts. Moreover, negligible values of LDH released both in osteoblasts monoculture on MGHA and on MGHA-Levo scaffolds are observed, proving no cytotoxic effect of both materials. Finally, results from MGHA-Levo scaffolds indicate a high efficiency of the system for keeping preosteoblast viability in co-culture conditions with bacteria.

### 3.5. *In vitro* biocompatibility studies of levofloxacin dosages

In an ideal delivery system, biocompatibility represents a basis ground of requirements to be combined with the drug antimicrobial effectiveness and adequate drug release kinetics, originating true multifunctional platforms for tissue regeneration. Biocompatibility studies should be carried out with the cell types with which the sys-

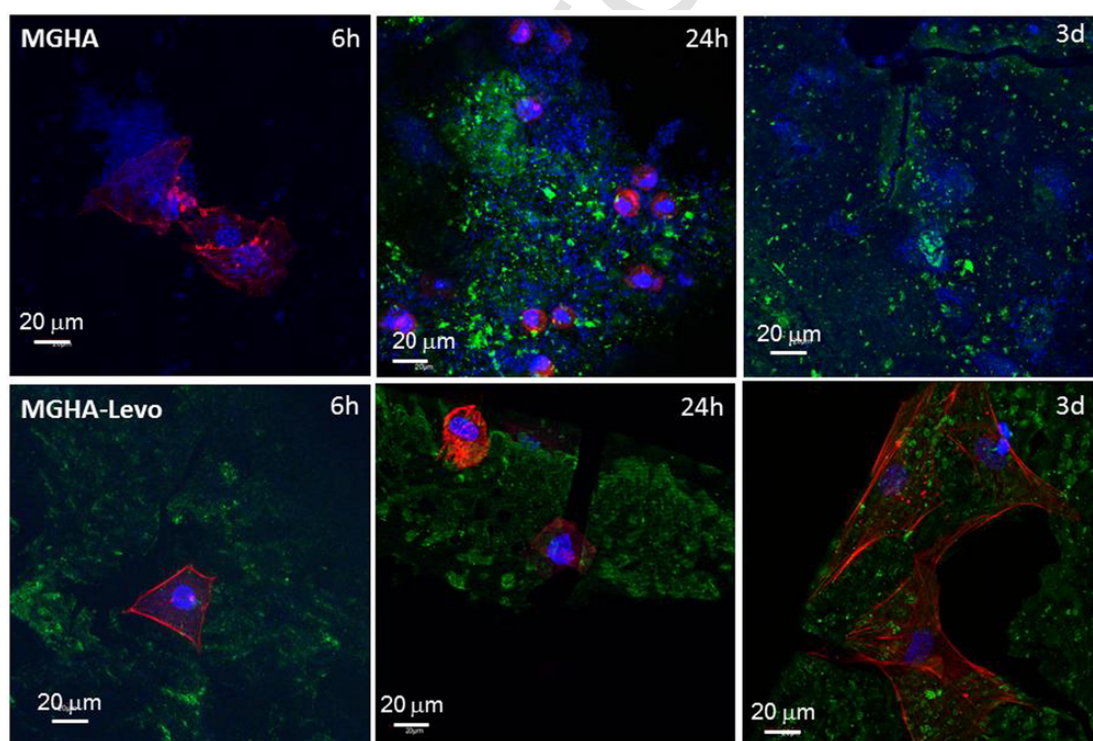


**Fig. 5.** *In vitro* competitive co-culture MC3T3-E1/*S. aureus* after 6h, 24h and 3 days of incubation onto MGHA and MGHA-Levo 3D scaffolds. Material refraction in green, preosteoblastic nuclei and bacteria in blue (DAPI) and actin-fibrous of preosteoblast cytoplasm in red (phalloidin).



tem comes into contact, analyzing the effects produced by the material physicochemical characteristics and the concentration of antimicrobial agent released. Recently, MGHA scaffolds have demonstrated excellent properties as highly bioactive behavior, enhanced biocompatibility, no induction of inflammatory response as well as good preosteoblast adhesion, colonization, proliferation and differentiation (supporting information, Fig. S1). These properties together with the results of Levo release shown in this study, suggest their great potential as multifunctional biomaterials for both bone tissue engineering and local drug delivery systems. Since Levo dose released from MGHA-Levo scaffolds is always higher than MIC for *S. aureus*, is important to evaluate possible cytotoxic effects caused by it on human Saos-2 osteoblasts. This cell type was cultured for 24 h in the presence of medium containing the Levo dose released at pH 7.4, after 3 and 24 h. Specifically, studied doses were of 1.8 µg/mL and 7.7 µg/mL, respectively, which corresponding to the maxim doses of Levo released. Note that, the Levo dose released to the characteristic pH of infection (pH 5.5) is 7.5 µg/mL, similar to the maximum dose assayed in these biocompatibility studies.

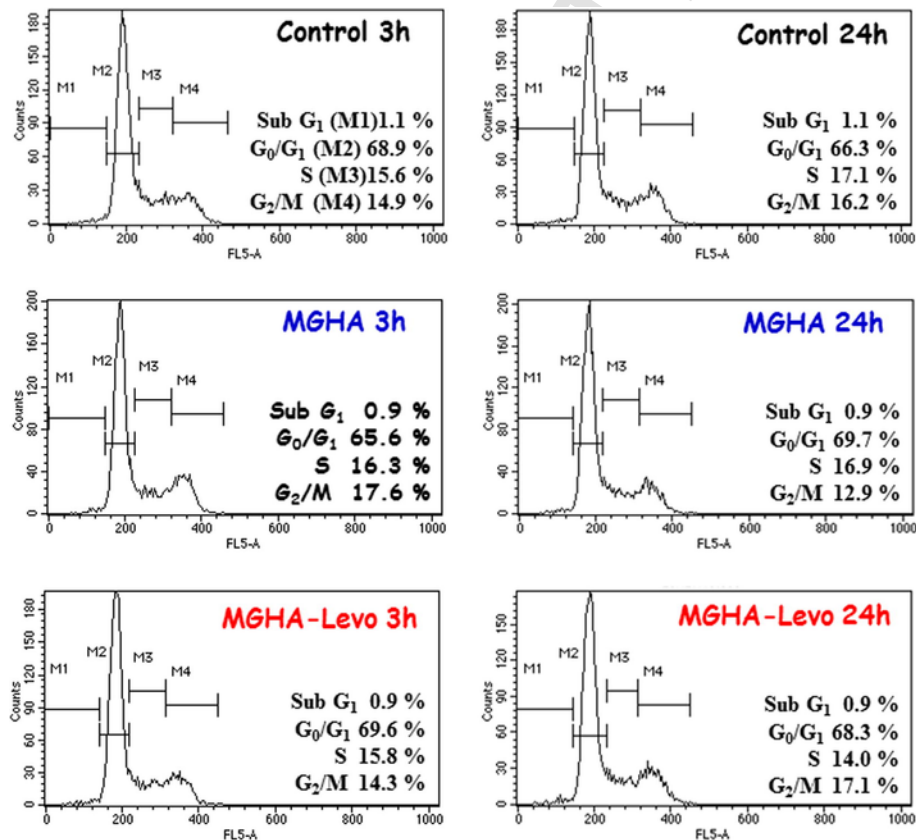
Fig. 6 shows the effects of Levo release on osteoblast cell cycle analyzed flow cytometry. The cell cycle phases G<sub>0</sub>/G<sub>1</sub>, S and G<sub>2</sub>/M correspond to repose/cytoplasm growth, DNA replication and mitosis phase, respectively. SubG<sub>1</sub>, corresponding to DNA fragmentation, was used as indicative of apoptosis. As it can be observed, the Levo doses released after 3 and 24 h (1.8 µg/mL and 7.7 µg/mL, respectively) do not alter any phase of the cell cycle G<sub>0</sub>/G<sub>1</sub>, S and G<sub>2</sub>/M of human Saos-2 osteoblasts. Moreover, SubG<sub>1</sub> fraction indicates very

low levels of cell death by apoptosis in all the experimental conditions assayed.

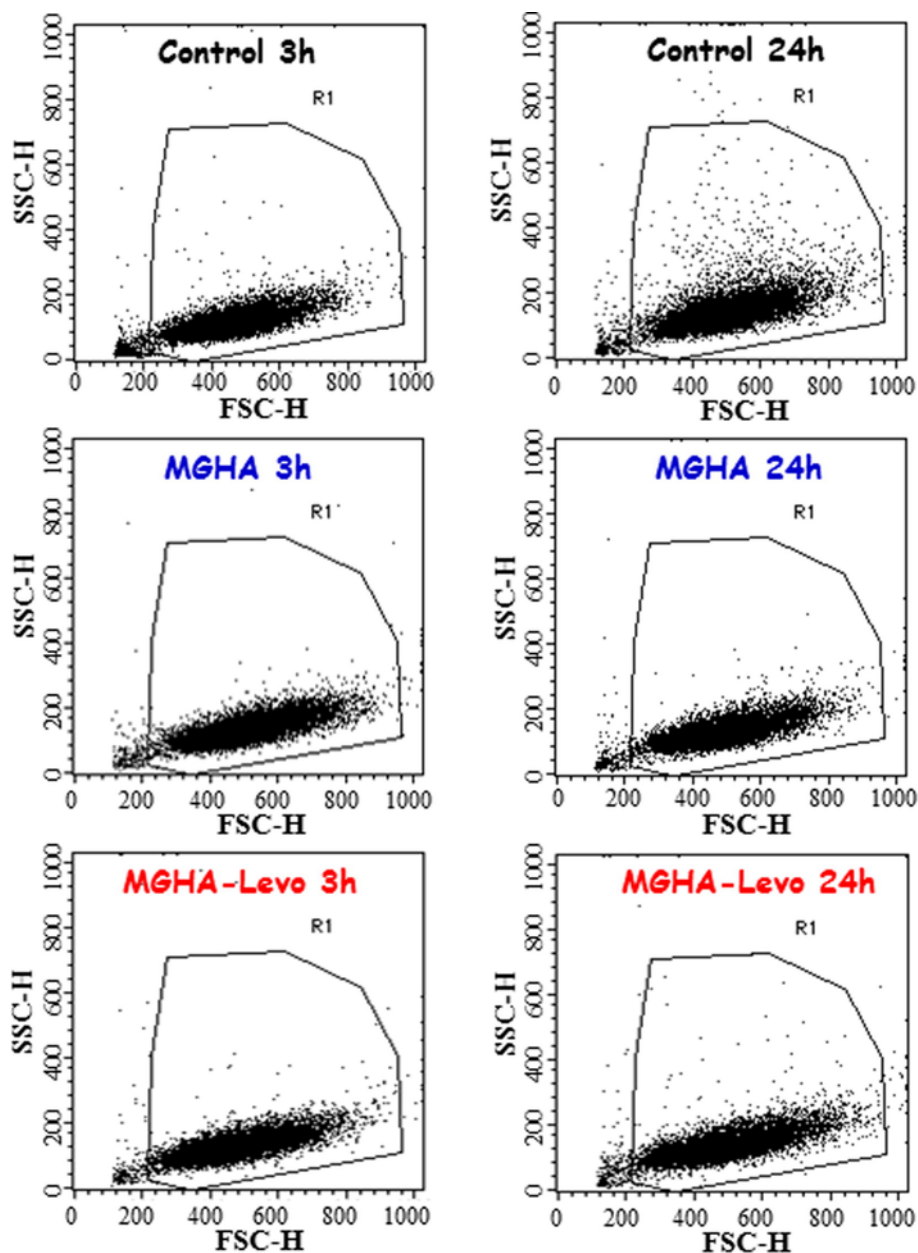
In order to know the possible cytotoxic effects on the cell size and internal complexity of Saos-2 osteoblasts, these cell parameters were evaluated by flow cytometry through FSC and 90° SSC light scatters, respectively, and are represented in Fig. 7. These properties are determined in part by plasma membrane, cytoplasm, mitochondria, pinocytic vesicles and lysosomes. The results highlight that no changes of these parameters were observed in Saos-2 osteoblasts cultured with the Levo doses studied.

Fig. 8 represents cell viability and apoptosis percentages, intracellular ROS content and cell proliferation values of Saos-2 osteoblasts after culture with DMEM containing the Levo dose released after 24 h, i.e. 7.7 µg/mL. No significant differences ( $p > .05$ ) are observed in viability and apoptosis of osteoblasts cultured with this dose, compared to control samples and osteoblasts cultured without Levo (MGHA sample). Therefore, Levo dose released after 24 h does not induce cellular dead. Moreover, the effects of this dose (7.7 µg/mL) on osteoblast proliferation and oxidative stress induced were also analyzed.

The results highlight that although the Levo dosage released after the 24 h is not cytotoxic, as it has been indicated above by the results of cell viability (Fig. 8), cell cycle phases (Fig. 6), cell size and internal complexity (Fig. 7), there is a slight but significant delay ( $p < .05$ ) in the osteoblasts proliferation after being cultured with medium containing the Levo dosage released after 24 h (Fig. 8). However, no significant differences ( $p > .05$ ) were found when the ROS content of osteoblasts cultured with the medium containing Levo is compared with



**Fig. 6.** Effects of Levo dose released from MGHA-Levo scaffolds after 3 and 24 h on the cell cycle of Saos-2 osteoblasts. Control: osteoblasts cultured in DMEM medium. MGHA 3h and MGHA 24h: osteoblasts cultured with medium which was in contact with MGHA scaffolds without Levo, after 3 and 24 h, respectively. MGHA-Levo 3h and MGHA-Levo 24h: osteoblasts cultured with.



**Fig. 7.** Effects of Levo dose released from MGHA-Levo scaffolds after 3 and 24 h on the light scattering properties of Saos-2 osteoblasts. Forward angle scatter (FCS, cell size) versus 90° side angle scatter (SSC, cell internal complexity) after each treatment. Control: osteoblasts cultured in DMEM medium. MGHA 3h and MGHA 24h: osteoblasts cultured with medium which was in contact with MGHA scaffolds without Levo after 3 h and 24 h, respectively. MGHA-Levo 3h and MGHA-Levo 24h: osteoblasts cultured with medium containing the Levo dose released from MGHA-Levo scaffolds after 3 h and 24 h, respectively.

the ROS values of control samples and Saos-2 osteoblasts cultured with supernatants of MGHA scaffolds without Levo (Fig. 8). Thus, these results confirm that the Levo dosage released after 24 h from MGHA scaffolds does not induce oxidative stress on Saos-2 osteoblasts.

#### 4. Conclusions

Tridimensional nanocomposite scaffolds with a pH-dependent and locally controlled Levo release have been designed. These 3D nanocomposite scaffolds exhibit a sustained Levo delivery at physio-

logical pH (pH 7.4), which increasing notably when pH decreases to characteristic values of bone infection process (pH 6.7 and pH 5.5). This pH-dependent Levo release is able to inhibit the *S. aureus* growth and to destroy a preformed *biofilm*, without cytotoxic effects on human osteoblasts. Moreover, *in vitro* co-culture assays with pre-osteoblasts and bacteria onto the 3D scaffold surface demonstrated an adequate cell colonization of the entire MGHA-Levo scaffold and its ability to eliminate bacterial contamination. Although further *in vivo* research is necessary, these findings reveal the possible potential of these 3D nanocomposite scaffolds to be used as therapeutic platforms for treatment and prevention of bone infection.

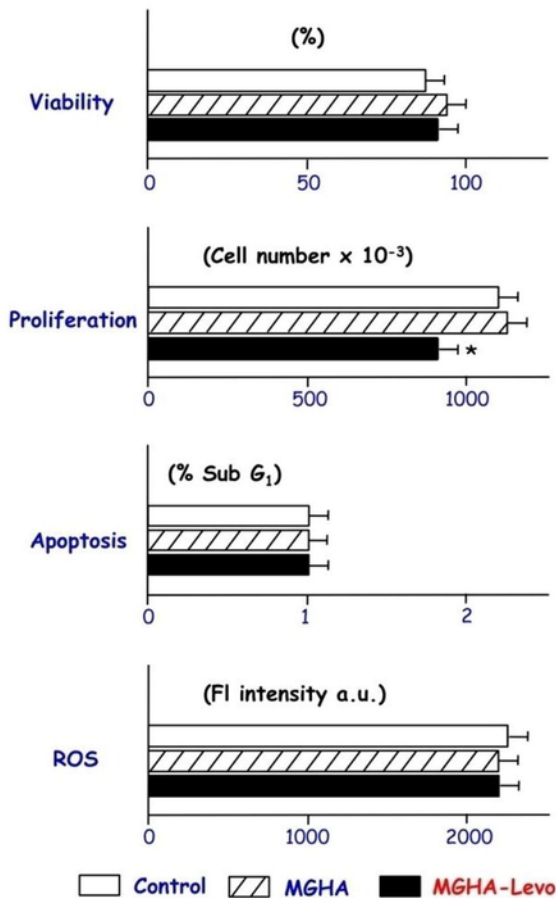


**Fig. 8.** Effects of Levo dose released from MGHA-Levo scaffolds after 24h on viability and apoptosis percentages, intracellular ROS content and proliferation values of Saos-2 osteoblasts. Control: osteoblasts cultured in DMEM medium. MGHA: osteoblasts cultured with medium which was in contact with MGHA scaffolds without Levo after 24h. MGHA-Levo: osteoblasts cultured with medium containing the Levo dose released from MGHA-Levo scaffolds after 24h. Statistical significance: \* $p < .05$ .

## Acknowledgments

MVR acknowledges funding from the European Research Council (Advanced Grant VERDI; ERC-2015-AdG Proposal No.694160). The author also thanks to Spanish MINECO (MAT2013-43299-R, MAT2015-64831-R, MAT2016-75611-R AEI/FEDER, UE). The authors wish to thank the ICTS Centro Nacional de Microscopia Electrónica (Spain), CAI X-ray Diffraction, CAI NMR, CAI Flow Cytometry and Fluorescence Microscopy of the Universidad Complutense de Madrid (Spain) for the assistance.

## Appendix A. Supplementary data

Supplementary data associated with this article can be found, in the online version, at <https://doi.org/10.1016/j.actbio.2017.11.009>.

## References

- [1] D.P. Lew, F.A. Waldvogel, Osteomyelitis, *Lancet* 364 (2004) 369–379.
- [2] I.G. Sia, E.F. Berbari, Infection and musculoskeletal conditions: osteomyelitis, *Best. Pract. Res. Clin. Rheumatol.* 20 (2006) 1065–1081.
- [3] J. Vila, A. Soriano, J. Mensa, Molecular basis of microbial adherence to prosthetic materials. Role of biofilms in prosthesis-associated infection, *Enferm. Infect. Microbiol. Clin.* 26 (2008) 48–54.

- [4] A.G. Gristina, M. Oga, L.X. Webb, C.D. Hobgood, Adherent bacterial colonization in pathogenesis of osteomyelitis, *Science* 228 (1985) 990–993.
- [5] C.R. Arciola, D. Campoccia, P. Speziale, L. Montanaro, J.W. Costerton, Biofilm formation in *Staphylococcus* implant infections. A review of molecular mechanisms and implications for biofilm-resistant materials, *Biomaterials* 33 (2012) 5967–5982.
- [6] K.J. Bozic, M.D. Ries, The impact of infection after total hip arthroplasty on hospital and surgeon resource utilization, *J. Bone Joint Surg. Am.* 87 (2005) 1746–1751.
- [7] D. Campoccia, L. Montanaro, C.R. Arciola, The significance of infection related to orthopedic devices and issues of antibiotic resistance, *Biomaterials* 27 (2006) 2331–2339.
- [8] J.A. Shuford, J.M. Steckelberg, Role of oral antimicrobial therapy in the management of osteomyelitis, *Curr. Opin. Infect. Dis.* 16 (2003) 515–519.
- [9] B. Parsons, E. Strauss, Surgical management of chronic osteomyelitis, *Am. J. Surg.* 188 (2004) 57–66.
- [10] R. Haidar, A. Der Boghossian, B. Atiyeh, Duration of post-surgical antibiotics in chronic osteomyelitis: empiric or evidence-based?, *Int. J. Infect. Dis.* 14 (2010) 752–758.
- [11] A.H. Simpson, M. Deakin, J.M. Latham, The effect of the extent of surgical resection on infection-free survival, *J. Bone Joint Surg. Br.* 83 (2001) 403–407.
- [12] T. Dvir, B.P. Timko, D.S. Kohane, R. Langer, Nanotechnological strategies forengineering complex tissues, *Nat. Nanotechnol.* 6 (2011) 13–22.
- [13] V. Guarino, M.G. Raucci, A. Ronca, V. Cirillo, L. Ambrosio, Multifunctional scaffolds for bone regeneration. Part II: biomaterial substitute scaffolds and implants for bone repair, In: *Bone Substitute Biomaterials*, 2014, pp. 95–117, ISBN: 978-0-85709-497-1.
- [14] C. Wu, Y. Zhou, M. Xu, P. Han, L. Chen, J. Chang, Y. Xiao, Copper-containing mesoporous bioactive glass scaffolds with multifunctional properties of angiogenesis capacity, osteostimulation and antibacterial activity, *Biomaterials* 34 (2013) 422–433.
- [15] H. Naderi, M.M. Matin, A.R. Bahrami, Critical issues in tissue engineering: biomaterials, cell sources, angiogenesis, and drug delivery systems, *J. Biomater. Appl.* 26 (2011) 383–417.
- [16] D. Campoccia, L. Montanaro, C.R. Arciola, A review of the clinical implications of anti-infective biomaterials and infection-resistant surfaces, *Biomaterials* 34 (2013) 8018–8029.
- [17] C.L. Huang, W.L. Lee, J.S.C. Loo, Drug-eluting scaffolds for bone and cartilage regeneration, *Drug Discov. Today* 19 (2014) 714–724.
- [18] S. Bagherifard, Mediating bone regeneration by means of drug eluting implants: from passive to smart strategies, *Mater. Sci. Eng. C* 71 (2017) 1241–1252.
- [19] D. Campoccia, L. Montanaro, P. Speziale, C.R. Arciola, Antibiotic-loaded biomaterials and the risk for the spread of antibiotic resistance following their prophylactic and therapeutic clinical use, *Biomaterials* 31 (2010) 6363–6377.
- [20] C.R. Rathbone, J.D. Cross, K.V. Brown, C.K. Murray, J.C. Wenke, Effect of various concentrations of antibiotics on osteogenic cell viability and activity, *J. Orthop. Res.* 29 (2011) 1070–1074.
- [21] S. Mura, J. Nicolas, P. Couvreur, Stimuli-responsive nanocarriers for drug delivery, *Nat. Mater.* 12 (2013) 991–1003.
- [22] S.K. Nandi, S. Bandyopadhyay, P. Das, I. Samanta, P. Mukherjee, S. Roy, B. Kundu, Understanding osteomyelitis and its treatment through local drug delivery system, *Biotechnol. Adv.* 34 (2016) 1305–1317.
- [23] C.C. de Carvalho, Biofilms: recent developments on an old battle, *Recent Pat. Biotechnol.* 1 (2007) 49–57.
- [24] P.D. Fey, M.E. Olson, Current concepts in biofilm formation of *Staphylococcus epidermidis*, *Future Microbiol.* 5 (2010) 917–933.
- [25] D. Dimakopoulou-Papazoglou, A. Lianou, K.P. Koutsoumanis, Modelling biofilm formation of *Salmonella enterica* ser. Newport as a function of pH and water activity, *Food Microbiol.* 53 (2016) 76–81.
- [26] M. Cicuendez, M.T. Portolés, I. Izquierdo-Barba, M. Vallet-Regí, New nanocomposite system with nanocrystalline apatite embedded into mesoporous bioactive glass, *Chem. Mater.* 24 (2012) 1100–1106.
- [27] M. Cicuendez, M. Malmsten, J.C. Doadrio, M.T. Portolés, I. Izquierdo-Barba, M. Vallet-Regí, Tailoring hierarchical meso–macroporous 3D scaffolds: from nano to macro, *J. Mater. Chem. B* 2 (2014) 49–58.
- [28] M. Cicuendez, P. Portolés, M. Montes-Casado, I. Izquierdo-Barba, M. Vallet-Regí, M.T. Portolés, Effects of 3D nanocomposite bioceramic scaffolds on the immune response, *J. Mater. Chem. B* 2 (2014) 3469–3479.
- [29] J.H. Shim, M.J. Kim, J.Y. Park, R.G. Pati, Y.P. Yun, S.E. Kim, H.R. Song, D.W. Cho, Three-dimensional printing of antibiotics-loaded poly-epsilon-caprolactone/poly(lactic-co-glycolic acid) scaffolds for treatment of chronic osteomyelitis, *Tissue Eng. Regen. Med.* 12 (2015) 283–293.
- [30] Y. Yang, S.B. Yang, Y.G. Wang, Z.F. Yu, H.Y. Ao, H.B. Zhang, L. Qin, O. Guillaume, D. Eglín, R.G. Richards, T.T. Tang, Anti-infective efficacy, cytocompatibility and biocompatibility of a 3D-printed osteoconductive composite scaffold functionalized with quaternized chitosan, *Acta Biomater.* 46 (2016) 112–128.
- [31] R.N. Greenberg, M.T. Newman, S. Shariaty, R.W. Pectol, Ciprofloxacin, lomefloxacin or levofloxacin as treatment for chronic osteomyelitis, *Antimicrob. Agents Chemother.* 44 (2000) 164–166.

- [32] H.A. Okerin, I.M. Arhewoh, Analytical profile of fluoroquinolone antibacterials I. Ofloxacin, *Africa J. Biotech.* 7 (2008) 670–680.
- [33] Y. Wang, W.R.G. Baeyens, C. Huang, G. Fei, L. Hem, J. Ouyang, Enhanced separation of seven quinolones by capillary electrophoresis with silica nanoparticles as additive, *Talanta* 7 (2009), 1674–1667.
- [34] E.P. Barrett, L.G. Joyner, P.P. Halenda, The determination of pore volume and area distributions in porous substances. I. Computations from nitrogen isotherms, *J. Am. Chem. Soc.* 73 (1951) 373–380.
- [35] M. Cicuéndez, I. Izquierdo-Barba, M.T. Portolés, M. Vallet-Regí, Biocompatibility and levofloxacin delivery of mesoporous materials, *Eur. J. Pharm. Biopharm.* 84 (2013) 115–124.
- [36] I. Izquierdo-Barba, J.M. García-Martín, R. Álvarez, A. Palmero, J. Esteban, C. Pérez-Jorge, D. Arcos, M. Vallet-Regí, Nanocolumnar coatings with selective behavior towards osteoblast and *Staphylococcus aureus* proliferation, *Acta Biomater.* 15 (2015) 20–28.
- [37] J. Josse, F. Velard, S.C. Gangloff, *Staphylococcus aureus* vs. osteoblast: relationship and consequences in osteomyelitis, *Front. Cell. Infect. Microbiol.* 5 (2015) 85.
- [38] A.H. Nguyen, S. Kim, W.J. Maloney, J.C. Wenke, Y. Yanga, Effect of Coadministration of Vancomycin and BMP-2 on Cocultured *Staphylococcus aureus* and W-20-17 Mouse Bone Marrow Stromal Cells In Vitro, *Antimicrob. Agents Chemother.* 56 (2012) 3776–3784.
- [39] H. Sudo, H.A. Kodama, Y. Amagai, S. Yamamoto, S. Kasai, In vitro differentiation and calcification in a new clonal osteogenic cell line derived from newborn mouse calvaria, *J. Cell Biol.* 96 (1983) 191–198.
- [40] W.N. Addison, V. Nelea, F. Chicatun, Y.C. Chien, N. Tran-Khanh, M.D. Buschmann, S.N. Nazhat, M.T. Kaartinen, H. Vali, M.M. Tecklenburg, R.T. Franceschi, M.D. McKee, Extracellular matrix mineralization in murine MC3T3-E1 osteoblast cultures: an ultrastructural, compositional and comparative analysis with mouse bone, *Bone* 71 (2015) 244–256.
- [41] L. Fassina, L. Visai, L. Asti, F. Benazzo, P. Speziale, M.C. Tanzi, G. Magenes, Calcified matrix production by SAOS-2 cells inside a polyurethane porous scaffold, using a perfusion bioreactor, *Tissue Eng.* 11 (2005) 685–700.
- [42] M. Vallet-Regí, M. Manzano, J.M. González-Calbet, E. Okunishid, Evidence of drugs confinement into silica mesoporous matrices by Stem CS Corrected Microscopy, *Chem. Commun.* 46 (2010) 2956–2958.
- [43] Y. Zhang, Z. Zhi, T. Jiant, Z. Wang, S. Wang, Spherical mesoporous silica nanoparticles for loading and release of poorly water-soluble drug telmisartan, *J. Control. Release* 145 (2010) 257–263.
- [44] M. Colilla, M.L. Ruiz-González, M. Martínez-Carmona, J.M. González-Calbet, S. Sánchez-Salcedo, M. Vallet-Regí, A novel zwitterionic bioceramic with dual antibacterial capability, *J. Mater. Chem. B* 2 (2014) 5639–5650.
- [45] R. García-Alvarez, I. Izquierdo-Barba, M. Vallet-Regí, 3D scaffold with effective multidrug sequential release against bacteria biofilm, *Acta Biomater.* 49 (2017) 113–126.
- [46] C. Hong, Ch. Liabo-bin, L. Yan-song, X. Han, W. Hui, Poly-D, L-lactide and levofloxacin-blended beads: a sustained local releasing system to treat osteomyelitis, *J. Appl. Poly. Sci.* 124 (2012) 3678–3684.
- [47] D. Molina-Manso, G. Del Prado, A. Ortiz-Perez, M. Manrubia-Cobo, E. Gómez-Barrena, J. Esteban Cordero-Ampuero, In vitro susceptibility to antibiotics of staphylococci in biofilms isolated from orthopaedic infections, *Int. J. Antimicrob. Agents* 41 (2013) 521–523.